Ferrimagnetism and single-particle excitations in a periodic Anderson model on the honeycomb lattice

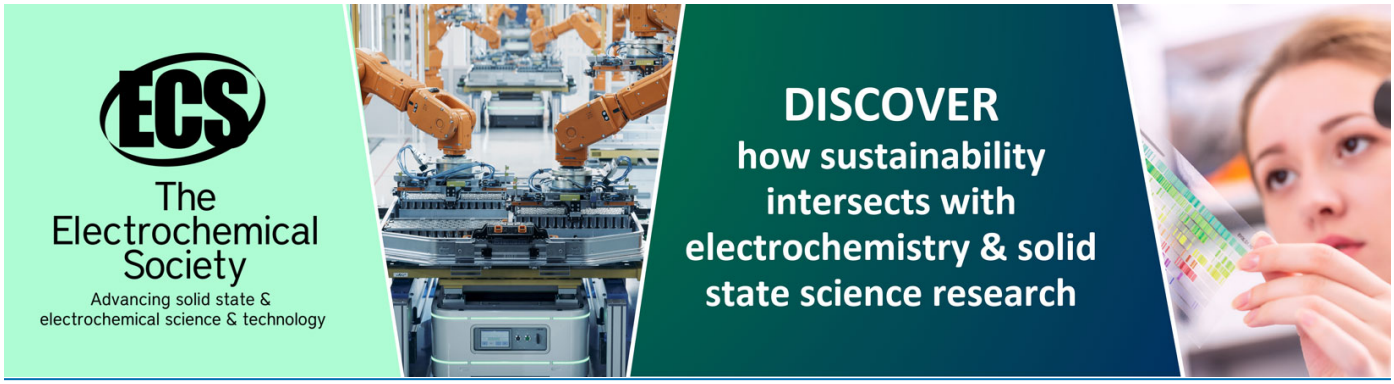

Journal of Physics: Conference Series **603** (2015) 012024 doi:10.1088/1742-6596/603/1/012024

Ferrimagnetism and single-particle excitations in a periodic Anderson model on the honeycomb lattice

Kazuhiro Seki[1], Tomonori Shirakawa[1,2], Qinfang Zhang[3], Tao Li[4], and Seiji Yunoki[1,2,5]

[1] Computational Condensed Matter Physics Laboratory, RIKEN, Wako, Saitama 351-0198, Japan
[2] Computational Materials Science Research Team, RIKEN Advanced Institute for Computational Science (AICS), Kobe Hyogo 650-0047, Japan
[3] Key Laboratory for Advanced Technology in Environmental Protection of Jiangsu Province, Yancheng Institute of technology,Yancheng 224051, China
[4] Department of Physics, Renmin University of China, Beijing, 100872, China
[5] Computational Quantum Matter Research Team, RIKEN Center for Emergent Matter Science (CEMS), Wako, Saitama 351-0198, Japan

E-mail: kazuhiro.seki@riken.jp

Abstract. By using the variational cluster approximation and cluster perturbation theory, we investigate the magnetism and single-particle excitations of a periodic Anderson model on the honeycomb lattice as an effective model for the single-side hydrogenated graphene, namely, graphone. We calculate the magnetic moment as a function of U (Coulomb interaction on impurity sites) with showing that the ground state is ferrimagnetic for any $U > 0$. We then calculate the single-particle excitations and show that the single-particle excitations are gapless and exhibit quadratic dispersion relation near the Fermi energy.

1. Introduction

Recently, a series of hydrogenated graphene [1, 2] attracts increasing attention because of its potential rich physics. A first-principles calculation based on density functional theory (DFT) has predicted that the single-side hydrogenated graphene, called graphone, becomes a ferromagnetic semiconductor with a small indirect gap [3]. Other DFT based study has suggested that the single-side hydrogenated and fluorinated graphenes can be a quantum spin liquid [4]. Possible increase of the spin-orbit coupling due to the sp^3 lattice distortion has been also discussed [5, 6]. However, electron correlation effects on the hydrogenated graphene beyond the DFT based calculations have not been investigated so far.

Here, we employ the variational cluster approximation (VCA) [7] and the cluster perturbation theory (CPT) [8] to investigate electron correlation effects on graphone by modeling it as a half-filled periodic Anderson model on the honeycomb lattice. We find that the ground state is ferrimagnetic (FM). The calculation of the magnetic moment as a function of electron correlation U at zero temperature shows that the magnetic moment in the weak-coupling region is naturally related to the flat-band FM. We also calculate the single-particle excitations and show that the low-energy excitations display the gapless quadratic dispersion.

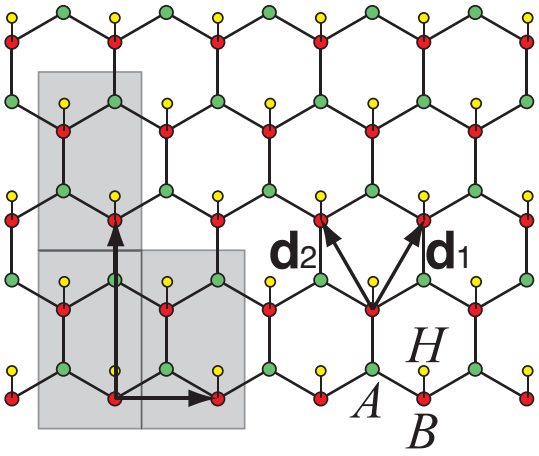

Figure 1. The periodic Anderson model on the honeycomb lattice. Carbon sites on A- and B-sublattices are denoted as green and red circles, respectively, and hydrogen sites are denoted as yellow circles. The shaded regions represent the 4-site (6-orbital) clusters used in the VCA and the CPT calculations. The arrows indicate primitive translational vectors for the cluster. The primitive translational vectors of the honeycomb lattice are also denoted by $\mathbf{d}_1$ and $\mathbf{d}_2$.

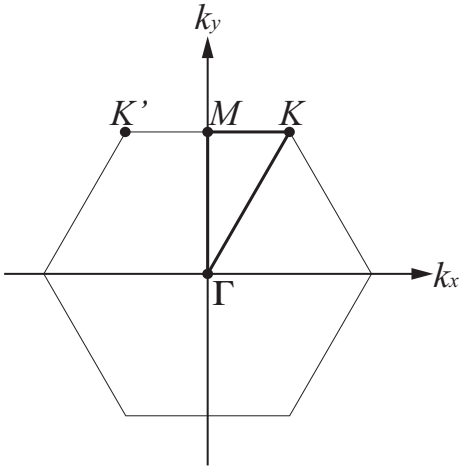

Figure 2. The Brillouin zone of the honeycomb lattice. Γ, M, K, and K' points are denoted as dots. Here $\Gamma = (0,0)$ and $M = 4\pi/3(0,\sqrt{3}/2)$. The thick triangle connecting Γ, M, and K points represents the momentum path used in Figs. 3(a) and (b).

2. Model

2.1. Periodic Anderson model

We consider a periodic Anderson model on the honeycomb lattice defined as

$$\mathcal{H} = \mathcal{H}_0 + \epsilon_H \sum_{i,\sigma} n_{i\sigma H} + U \sum_i n_{i\uparrow H} n_{i\downarrow H}, \tag{1}$$

where

$$\mathcal{H}_0 = -t \sum_{\langle i,j\rangle,\sigma} c^\dagger_{i\sigma A} c_{j\sigma B} - t \sum_{i,\sigma} c^\dagger_{i\sigma A} c_{i\sigma B} + t_{sp} \sum_{i,\sigma} c^\dagger_{i\sigma B} c_{i\sigma H} + \text{H.c.}, \tag{2}$$

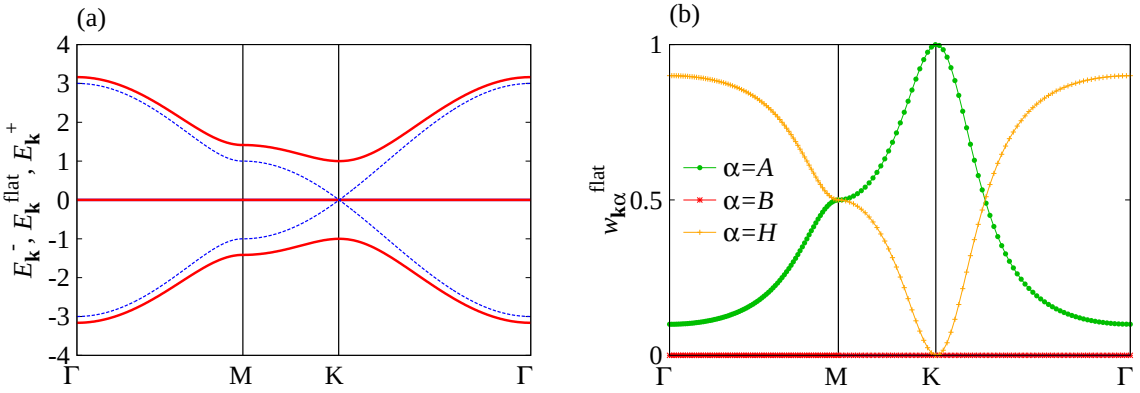

Figure 3. (a) The non-interacting tight-binding dispersion relations $E^{-}_{\mathbf{k}}$, $E^{\rm flat}_{\mathbf{k}}$, and $E^{+}_{\mathbf{k}}$ with $t_{sp}/t = 1$ (red solid lines). The non-interacting tight-binding dispersion relations for pure graphene model are also shown (blue dashed lines). (b) The orbital-resolved spectral weights $w^{\rm flat}_{\mathbf{k}A}$, $w^{\rm flat}_{\mathbf{k}B}$, and $w^{\rm flat}_{\mathbf{k}H}$ for the flat band $E^{\rm flat}_{\mathbf{k}}$ in the non-interacting limit with $t_{sp}/t = 1$. The results are shown along the path in the momentum space given in Fig. 2.

$c^{\dagger}_{i\sigma\alpha}$ is the electron creation operator with spin $\sigma\,(=\uparrow,\downarrow)$ and orbital $\alpha\,(=A,B,H)$ in the i-th unit cell, and $n_{i\sigma\alpha} = c^{\dagger}_{i\sigma\alpha}c_{i\sigma\alpha}$. Here, orbital A (B) denotes carbon p_z orbital on A (B)-sublattice of the honeycomb lattice and orbital H indicates hydrogen s orbital [see Fig. 1(a)]. The sum in the first term of Eq. (2), indicated by $\langle i,j\rangle$, runs over all pairs of nearest-neighboring unit cells. The first and second terms represent the hopping between the nearest-neighboring carbon sites with the hopping integral t, forming the conduction bands. t_{sp} is the hybridization between the hydrogen "impurity" site and the carbon site on B-sublattice. ϵ_H is the on-site potential energy and U is the on-site Coulomb repulsion of the hydrogen sites. This is the simplest model for graphone by implicitly assuming the hopping integral t in Eq. (2) as the renormalized one due to electron correlations in carbon sites [9, 10]. We consider the particle-hole symmetric case with $\epsilon_H = -U/2$, in which the electron density n is exactly 1 for any U values. We also set $t = t_{sp} = 1$ and $\hbar = k_B = 1$.

2.2. Non-interacting limit

In the non-interacting case with $\epsilon_H = 0$, the Hamiltonian in the momentum space can be written as

$$\mathcal{H}_0 = \sum_{\mathbf{k},\sigma} \left(c^{\dagger}_{\mathbf{k}\sigma A} c^{\dagger}_{\mathbf{k}\sigma B} c^{\dagger}_{\mathbf{k}\sigma H} \right) \begin{pmatrix} 0 & \gamma_{\mathbf{k}} & 0 \\ \gamma^{*}_{\mathbf{k}} & 0 & t_{sp} \\ 0 & t_{sp} & 0 \end{pmatrix} \begin{pmatrix} c_{\mathbf{k}\sigma A} \\ c_{\mathbf{k}\sigma B} \\ c_{\mathbf{k}\sigma H} \end{pmatrix}, \tag{3}$$

where $c^{\dagger}_{\mathbf{k}\sigma\alpha}$ is the Fourier transform of the real-space creation operator and

$$\gamma_{\mathbf{k}} = -t \left(1 + e^{i\mathbf{k}\cdot\mathbf{d_1}} + e^{i\mathbf{k}\cdot\mathbf{d_2}} \right) \tag{4}$$

is the matrix element between carbon p_z orbitals on A and B sublattices. Here,

$$\mathbf{d}_1 = \left(\frac{1}{2}, \frac{\sqrt{3}}{2} \right), \quad \mathbf{d}_2 = \left(-\frac{1}{2}, \frac{\sqrt{3}}{2} \right), \tag{5}$$

are primitive translational vectors of the honeycomb lattice (Fig. 1). Notice that, at $\mathbf{k} = K$ and K' points defined as (see also Fig. 2)

$$K = \frac{4\pi}{3}\left(\frac{1}{2}, \frac{\sqrt{3}}{2}\right), \quad K' = \frac{4\pi}{3}\left(-\frac{1}{2}, \frac{\sqrt{3}}{2}\right), \tag{6}$$

$\gamma_{\mathbf{k}}$ becomes zero, i.e., $\gamma_K = \gamma_{K'} = -t(1 + e^{2\pi i/3} + e^{4\pi i/3}) = 0$. The non-interacting tight-binding band dispersion relations are given as

$$E^{\rm flat}_{\mathbf{k}} = 0, \tag{7}$$

$$E^{\pm}_{\mathbf{k}} = \pm\sqrt{|\gamma_{\mathbf{k}}|^2 + t_{sp}^2}. \tag{8}$$

We thus find that $\mathcal{H}_0$ has a flat band just at the Fermi energy $E_{\rm F} = 0$. It also should be noted that the massless Dirac electronic dispersion is absent in the non-interacting limit [see Fig. 3(a)]. The orbital-resolved spectral weights for the flat band are given as

$$w^{\rm flat}_{\mathbf{k}A} = \langle\phi^{\rm flat}_{\mathbf{k}}|c^{\dagger}_{\mathbf{k}A\sigma}c_{\mathbf{k}A\sigma}|\phi^{\rm flat}_{\mathbf{k}}\rangle = \frac{t_{sp}^2}{|\gamma_{\mathbf{k}}|^2 + t_{sp}^2} \tag{9}$$

$$w^{\rm flat}_{\mathbf{k}B} = \langle\phi^{\rm flat}_{\mathbf{k}}|c^{\dagger}_{\mathbf{k}B\sigma}c_{\mathbf{k}B\sigma}|\phi^{\rm flat}_{\mathbf{k}}\rangle = 0 \tag{10}$$

$$w^{\rm flat}_{\mathbf{k}H} = \langle\phi^{\rm flat}_{\mathbf{k}}|c^{\dagger}_{\mathbf{k}H\sigma}c_{\mathbf{k}H\sigma}|\phi^{\rm flat}_{\mathbf{k}}\rangle = \frac{|\gamma_{\mathbf{k}}|^2}{|\gamma_{\mathbf{k}}|^2 + t_{sp}^2}, \tag{11}$$

where $|\phi^{\rm flat}_{\mathbf{k}}\rangle$ is the eigenstate of the flat band. Equations (9)-(11) indicate that the flat band consists of A and H orbitals, but not B orbital. In particular, the flat band at K (and K') point is solely consists of A orbital [see Fig. 3(b)].

The existence of the flat band Eq. (7) can be understood by recalling the Lieb's argument on bipartite lattices [11]. Namely, because of the imbalance of the number of sublattices, $\mathcal{H}_0$ has $|A| + |H| - |B|$ ($|\alpha|$: the number of α orbitals) zero eigenvalues, forming the flat band. This also explains why the wave functions with zero eigenvalues are contributed only from A and H orbitals, but not from B orbital. It should be also noted here that the tight-binding model considered here captures the characteristic features of the band structures for graphone obtained by a spin-unpolarized DFT calculation [4].

3. Methods

3.1. Variational cluster approximation

In order to investigate a possible symmetry breaking state, we employ the VCA [7] which is a cluster method formulated based on the self-energy-functional theory [12]. In the VCA, the original lattice is divided into disconnected finite-size clusters, and then variational parameters are introduced to examine possible symmetry breaking states. Here the two-body interaction term must be the same as the original one, whereas the one-body term can be changed [12]. The collection of these disconnected clusters is called "reference system" and its self-energy is used as a trial function for the grand-potential functional to be optimized based on the self-energy functional theory.

Here, we introduce, as a variational parameter, a uniform field h' on the hydrogen (impurity) sites [13] described as

$$\mathcal{H}_{h'} = h' \sum_i \left(n_{i\uparrow H} - n_{i\downarrow H}\right). \tag{12}$$

The reference system $\mathcal{H}_{\rm ref}$ considered is thus composed of a collection of disconnected finite size clusters as shown in Fig. 1(a), each cluster being described by $\mathcal{H}$ with no hopping terms between clusters (denoted as $\mathcal{H}_{\rm c}$), and $\mathcal{H}_{h'}$, i.e., $\mathcal{H}_{\rm ref} = \mathcal{H}_{\rm c} + \mathcal{H}_{h'}$.

In the VCA, the grand-potential functional per unit cell at zero temperature is given as [14]

$$\Omega = \frac{1}{L_{\rm c}}\Omega' - \frac{1}{NL_{\rm c}\pi}\int_0^\infty {\rm d}x \sum_\sigma \sum_{\tilde{\mathbf{k}}} \ln\left|\det\left(\boldsymbol{I} - \boldsymbol{V}_\sigma(\tilde{\mathbf{k}})\boldsymbol{G}'_\sigma(ix)\right)\right|. \tag{13}$$

where Ω' is the exact grand potential of the single cluster, $\tilde{\mathbf{k}}$ is the wave vector defined in the reduced Brillouin zone of the reference system, N is the number of clusters and $L_{\rm c}$ is the number of unit cells in a cluster. The exact single-particle Green's function of $\mathcal{H}_{\rm ref}$ is denoted as $\boldsymbol{G}'_\sigma(ix)$ and $\boldsymbol{V}_\sigma \equiv \boldsymbol{G}'^{-1}_{\sigma 0} - \boldsymbol{G}^{-1}_{\sigma 0}$ represents the difference between the one-body terms of $\mathcal{H}$ and $\mathcal{H}_{\rm ref}$. We employ the exact diagonalization technique to calculate $\boldsymbol{G}'_\sigma(ix)$ and Ω'. The FM state is obtained when a saddle point $\partial\Omega/\partial h'|_{h'=h^*} = 0$ with the lowest Ω is at $h^* \neq 0$. Notice that in this paper we focus on the physics at zero temperature.

3.2. Cluster perturbation theory

The CPT [8] is employed to obtain the translational invariant Green's function of the infinite systems. In the CPT, the single-particle Green's function $\mathcal{G}^{\alpha\beta}_\sigma(\mathbf{k},\omega)$ is given as

$$\mathcal{G}^{\alpha\beta}_\sigma(\mathbf{k},\omega) = \frac{1}{3L_c}\sum_{i,j}\left(\boldsymbol{G}'^{-1}_\sigma(\omega) - \boldsymbol{V}_\sigma(\mathbf{k})\right)^{-1}_{i\alpha,j\beta} e^{-i\mathbf{k}\cdot(\mathbf{r}_i - \mathbf{r}_j)}, \tag{14}$$

where $\mathbf{r}_i$ denotes the location of the i-th unit cell in the cluster. Here, the momentum $\mathbf{k}$ can take arbitrary value in the momentum space, and the frequency ω can take arbitrary value in the complex-frequency space. The single-particle spectral function for α orbital with spin σ is given as

$$A^{\alpha\alpha}_\sigma(\mathbf{k},\omega) = -\frac{1}{\pi}\Im\mathcal{G}^{\alpha\alpha}_\sigma(\mathbf{k},\omega + i\eta), \tag{15}$$

where η gives the Lorentzian broadening of the spectra.

4. Results

4.1. Ferrimagnetism

By calculating the grand-potential functional Ω as a function of h', we find that the FM state is stabilized for $U > 0$. We then calculate the magnetic moment per unit cell defined as

$$m_z = \sum_\alpha m_{z\alpha} \tag{16}$$

where $m_{z\alpha}$ is the magnetic moment of α orbital per unit cell which is given as [14]

$$m_{z\alpha} = \frac{1}{NL_{\rm c}\pi}\int_0^\infty {\rm d}x \sum_\sigma \sum_{\tilde{\mathbf{k}}} \sum_i \sigma_z \Re\left[\left(\boldsymbol{G}'^{-1}_\sigma(ix) - \boldsymbol{V}_\sigma(\tilde{\mathbf{k}})\right)^{-1}\right]_{i\alpha,i\alpha} \tag{17}$$

with σ_z being the z component of the Pauli matrices, i.e., $\sigma_z = 1(-1)$ for $\sigma = \uparrow (\downarrow)$. Figure 4 shows the calculated results of m_{zA}, m_{zB}, m_{zH}, and m_z as a function of U/t at zero temperature. We find that $m_z = 1$ within the numerical accuracy for any U. We also find that $m_{zA} > 0$, $m_{zB} < 0$, and $m_{zH} > 0$ as expected from the bipartite structure of the lattice. In the small U region, m_{zB} approaches to zero, whereas m_{zA} and m_{zH} approach to finite values in the non-interacting limit. Now let us consider the magnetic moment in the non-interacting limit. Since

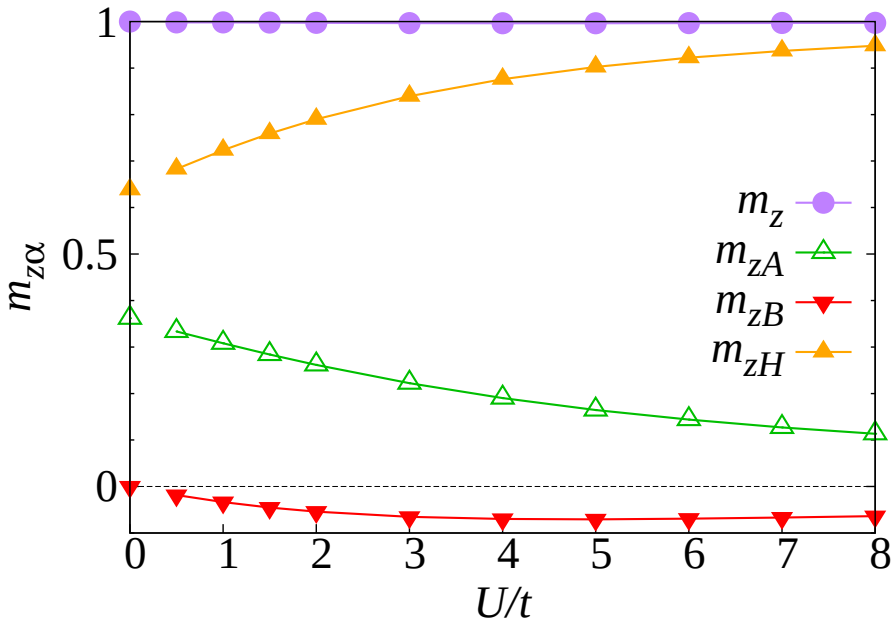

Figure 4. U-dependence of the orbital-resolved magnetic moments m_{zA}, m_{zB}, and m_{zH}, and the total magnetic moment m_z per unit cell. The magnetic moments in the non-interacting limit are also shown as symbols on the vertical axis at $U/t = 0$.

there exists the flat band at $E_{\rm F}$, the system is unstable against the FM long-range order for any $U > 0$. Assuming that the flat band is fully polarized in the non-interacting limit, the magnetic moments in the non-interacting limit can be calculated as [see Eqs. (9), (10), and (11)]

$$\lim_{U\to 0} m_{zA} = \frac{1}{L}\sum_{\mathbf{k}} \frac{t_{sp}^2}{|\gamma_{\mathbf{k}}|^2 + t_{sp}^2} \simeq 0.362, \tag{18}$$

$$\lim_{U\to 0} m_{zB} = 0, \tag{19}$$

$$\lim_{U\to 0} m_{zH} = \frac{1}{L}\sum_{\mathbf{k}} \frac{|\gamma_{\mathbf{k}}|^2}{|\gamma_{\mathbf{k}}|^2 + t_{sp}^2} \simeq 0.638, \tag{20}$$

where L is the number of unit cells and the numerical values are for $t = t_{sp} = 1$. The magnetic moments calculated by the VCA indeed approach to those values with decreasing U. Notice that a similar model on the square lattices has been recently studied in Ref. [15].

In the large U region, the magnetic moment becomes dominated by H orbital. Note that, in the strong coupling limit, an electron in each hydrogen site is completely localized and the RKKY interaction [16, 17, 18] between these localized spins is ferromagnetic [19], which naturally induces the FM ground state.

4.2. Single-particle excitations

Figures 5(a)-(d) show the single-particle excitation spectra $A_\sigma^{\alpha\alpha}(\mathbf{k}, \omega)$ for momentum $\mathbf{k}$ around K point at $U/t = 4$. The low-energy single-particle excitations show quadratic dispersion relation around K point, indicating massive Dirac quasi-particle excitations. Although the dispersion

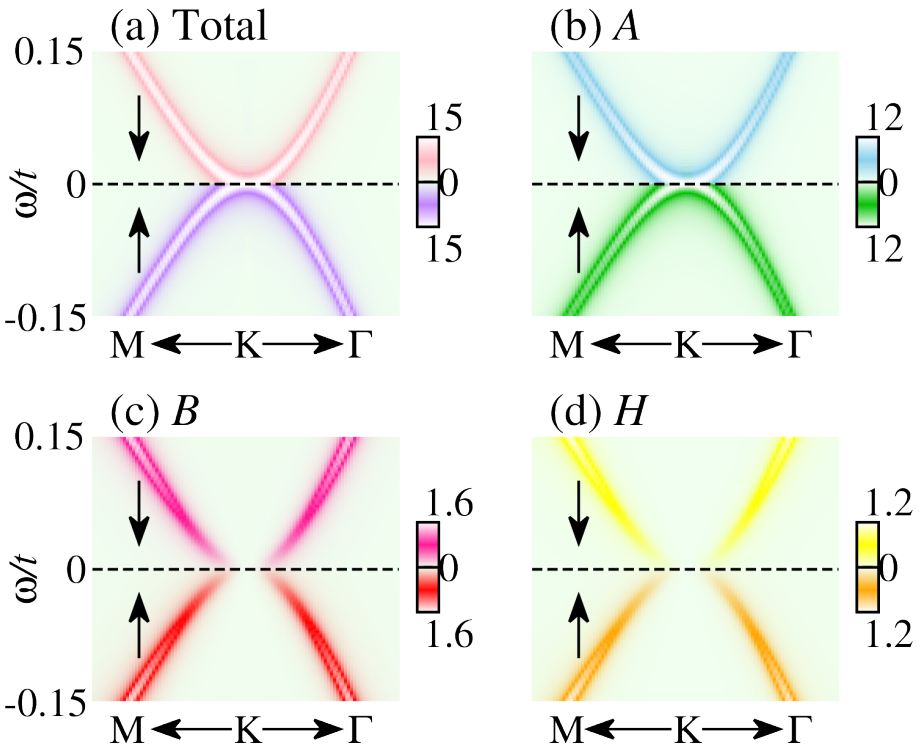

Figure 5. The single-particle excitations for $U/t = 4$ at the vicinity of K point near $E_{\rm F}$. (a) $A_\sigma(\mathbf{k},\omega) = \sum_\alpha A_\sigma^{\alpha\alpha}(\mathbf{k},\omega)$, (b) $A_\sigma^{AA}(\mathbf{k},\omega)$, (c) $A_\sigma^{BB}(\mathbf{k},\omega)$, and (d) $A_\sigma^{HH}(\mathbf{k},\omega)$. Here $\eta/t = 0.01$ is used. $A_\uparrow^{\alpha\alpha}(\mathbf{k},\omega)$ and $A_\downarrow^{\alpha\alpha}(\mathbf{k},\omega)$ are indicated with different colors. The region of momenta taken in the horizontal axis is 0.2π in the K-M (K-Γ) direction from K.

relation is massive, the single-particle gap is absent at K point. We also find that the A-orbital spectral weight at K point at $E_{\rm F}$ is finite even there exists the electron correlation U in H orbital, which also forms the flat band in the non-interacting limit. This is because the A orbital is completely decoupled from the H orbital at K point in the non-interacting limit [see Fig. 3(b)], thereby the electron correlation U on H orbital does not affect the spectrum of A orbital at K point. Therefore, the single-particle gap is absent at K point even at finite U. The same discussion holds for K' point. The single-particle excitation spectra in the FM state thus exhibit point-contact massive Dirac dispersion.

5. Summary

Using the VCA and the CPT, we have studied the magnetism and single-particle excitations of a half-filled periodic Anderson model at zero temperature. We have calculated the spontaneous magnetization as a function of electron correlation U. In the small U region, the calculated magnetic moments approach to those estimated from the flat-band ferrimagnetism. In the large U region, the H orbital gives the dominant contribution to the magnetic moment. Interestingly, the single-particle excitations in the FM state show a point-contact quadratic dispersion relation around the K and K' points. So far our study has been done at zero temperature in the magnetic state. Further study at finite temperatures in which the magnetic long-range order is destabilized will be reported elsewhere [20].

Acknowledgments
The computations have been done using the RIKEN Integrated Cluster of Clusters (RICC) facility. This work has been supported in part by Grant-in-Aid for Scientific Research from MEXT Japan under the grant Nos. 24740269 and 26800171 and by RIKEN iTHES Project and Molecular Systems. Q.Z. also acknowledges the National Natural Science Foundation of China (11204265), the Natural Science Foundation of Jiangsu Province (BK2012248) and the College Natural Science Research Project of Jiangsu Province (13KJ430007).

References
[1] Sofo J O, Chaudhari A S and Barber G D 2007 *Phys. Rev. B* **75** 153401
[2] Elias D C, Nair R R, Mohiuddin T M G, Morozov S V, Blake P, Halsall M P, Ferrari A C, Boukhvalov D W, Katsnelson M I, Geim A K and Novoselov K S 2009 *Science* **323** 610
[3] Zhou J, Wang Q, Sun Q, Chen X X, Kawazoe Y and Jena P 2009 *Nano Lett.* **9** 3867
[4] Rudenko A N, Keil F J, Katsnelson M I and Lichtenstein A I 2013 *Phys. Rev. B* **88** 081405(R)
[5] Castro Neto A H and Guinea f 2009 *Phys. Rev. Lett.* **103** 026804
[6] Gmitra M, Kochan D and Fabian J 2013 *Phys. Rev. Lett.* **110** 246602
[7] Potthoff M, Aichhorn M and Dahnken C 2003 *Phys. Rev. Lett.* **91** 206402
[8] Sénéchal D, Perez D and Pioro-Ladriere M 2000 *Phys. Rev. Lett.* **84** 522
[9] Sorella S, Otsuka Y and Yunoki S 2012 *Sci. Rep.* **2** 992
[10] Schuler M, Rosner M, Wehling T O, Lichtenstein A I and Katsnelson M I 2013 *Phys. Rev. Lett.* **111** 036601
[11] Lieb E H 1989 *Phys. Rev. Lett.* **62** 1201
[12] Potthoff M 2003 *Eur. Phys. J. B* **32** 429
[13] Horiuchi S, Kudo S, Shirakawa T and Ohta Y 2008 *Phys. Rev. B* **78** 155128
[14] Sénéchal D *e-print arXiv:0806.2690*
[15] Titvinidze I, Schwabe A and Potthoff M 2014 *Phys. Rev. B* **90** 045112
[16] Ruderman M A and Kittel C 1954 *Phys. Rev.* **96** 99
[17] Kasuya T 1956 *Prog. Theor. Phys.* **16** 45
[18] Yoshida K 1958 *Phys. Rev.* **106** 893
[19] Saremi S 2007 *Phys. Rev. B* **76** 184430
[20] Seki K, Shirakawa T, Zhang Q, Li T and Yunoki S *submitted*